Journal of Solid State Chemistry **146,** 418–427 (1999)
Article ID jssc.1999.8386, available online at http://www.idealibrary.com on IDEAL®

# Discontinuous Evolution of the Highly Distorted Orthorhombic Structure and the Magnetic Order in $LaMnO_{3\pm\delta}$ Perovskite

F. Prado, R. D. Sánchez,[1,2] A. Caneiro, M. T. Causa, and M. Tovar

*Centro Atómico Bariloche and Instituto Balseiro, Comisión Nacional de Energia Atómica and Universidad Nacional de Cuyo, 8400 San Carlos de Bariloche, Argentina*

Received February 5, 1999; in revised form April 29, 1999; accepted May 21, 1999

**In this work we present a systematic study of the crystallographic structure and the magnetic ordering of $LaMnO_{3\pm\delta}$ perovskites. Changing the oxygen composition within the range $2.995 < 3 \pm \delta < 3.140$, we found a $3 + \delta_1$ value ($3.04 < 3 + \delta_1 < 3.05$) which defines a boundary in the magnetic phase diagram $T$ vs $3 \pm \delta$. For $3 + \delta < 3 + \delta_1$, antiferromagnetic order is present in the samples with a small ferromagnetic component, while for large $3 + \delta$ values ($3 + \delta > 3 + \delta_1$) the samples are ferromagnetic. The transition from one region to the other is associated with a change in volume of around 1%.** © 1999 Academic Press

*Key Words:* **$LaMnO_3$; Jahn–Teller; weak ferromagnetism.**

## I. INTRODUCTION

The recent discovery of huge negative magnetoresistance near the Curie temperature, called colossal magnetoresistance (CMR) (1, 2), in lanthanum manganite doped with cations such as $M^{2+}$ ($M$ = Ca, Sr, Ba) has created renewed interest in the structural, magnetic, and electronic properties of these perovskites. The double-exchange mechanism (3, 4), present in these systems with $Mn^{3+}/Mn^{4+}$ ions and mobile carriers (5), plays an important role in the metallic and ferromagnetic characteristics (6) of these manganites. Nevertheless, this mechanism does not explain totally the CMR phenomena (7) and Millis *et al.* (8) proposed adding to it a polaron effect due to a strong electron–phonon coupling coming from a Jahn–Teller splitting of the $Mn^{3+}$ ion.

From pioneer experiments (9) it is known that the stoichiometric $LaMnO_3$ (where all the manganese ions are three-valent) is an orthorhombic structure with $A$-type antiferromagnetic (AFM) order. Early phenomenological explanation was made relating an orbital ordering as the origin of this magnetic configuration (10) with anisotropic $Mn^{3+}$–O–$Mn^{3+}$ superexchange interactions. This anisotropy is stabilized by a cooperative Jahn–Teller distortion (JTD) giving the O′-phase ($c/\sqrt{2} < a < b$). This static deformation produces a ferromagnetic (FM) ordering of all $Mn^{3+}$ within the $a$–$b$ planes, due to the superexchange effect between empty and occupied $e_g$ states. The ferromagnetic planes compensate one another by the dominant antiferromagnetic superexchange between two manganese with three half-filled $t_{2g}$ orbitals. The tilt of $MnO_6$ octahedra around the [010] axis causes an orthorhombic $D_{2h}^{16}$ superstructure with four unit formulae in the primitive cell, this being a second cooperative distortion that occurs in this crystalline structure. This process introduces an antisymmetric Dzialoshinski exchange coupling ($\mathbf{D_{ij}} \cdot \mathbf{S_i} \times \mathbf{S_j}$) giving weak canted spin ferromagnetism.

The cooperative JTD can be suppressed in several ways. One of them is when the temperature is raised and a phase transition takes place at $T_{JT}$ between the distorted orthorhombic phase (O′) and a pseudocubic one O ($a \leq c/\sqrt{2} < b$), making the $MnO_6$ octahedra nearly regular above $T_{JT}$. Recently, a systematic study of the magnetic susceptibility around this transition reported (11) a wide hysteresis of the susceptibility between heating and cooling runs which has been associated with the coexistence of two orthorhombic phases (O′ and O) (12). These data indicate that the transition between O′ and O phases is a first-order phase transition. At high temperatures another structural transition from an O phase to a rhombohedral (R) phase occurs (13).

At room temperature the cooperative JTD can be suppressed by substitution of the $Mn^{3+}$ by other three-valent ions as $Ga^{3+}$, $Ni^{3+}$, or $Co^{3+}$, producing a less distorted orthorhombic structure O with isotropic $Mn^{3+}$–O–$Mn^{3+}$ ferromagnetic interactions (14) or by an increase in the oxygen content (or $Mn^{4+}$) of the $LaMnO_{3+\delta}$ samples (15).

The magnetic phases of $LaMnO_{3+\delta}$ as a function of $3 + \delta$ and $T$ has been studied by several authors. While the pioneer work of de Gennes (5) proposes that the small amounts of $Mn^{4+}$ produce a canted spin arrangement,

PACS numbers: 75.30Vn; 75.30.Gw; 71.70.Ej

[1]Member of Carrera de Investigador CONICET, Argentina.
[2]To whom correspondence should be addressed. Fax: +54-2944-445299. e-mail: rodo@cab.cnea.gov.ar.



0022-4596/99 $30.00

other authors suggest a spiral spin state as the stable magnetic structure for these perovskites (16). Nevertheless, complex techniques such as neutron diffraction and Muon spin rotation are needed to clarify the fundamental magnetic phase.

The variation of oxygen in $LaMnO_{3\pm\delta}$ induces structural (17) and several magnetic transitions because the oxygen content allows one to change the $Mn^{4+}/Mn^{3+}$ ratio in a wide range. Therefore, this is a very attractive system for studying the correlation between structural and magnetic properties. Some points of consensus have been highlighted in previous papers: as $3+\delta$ increases, the oxygen excess corresponds to equal amounts of Mn and La vacancies in the perovskite structure (18); the cooperative JTD decreases and the magnetism of the system evolves from antiferromagnetic to ferromagnetic (19, 21). However, most of the magnetic and structural studies were carried out only with a few samples of controlled oxygen content, leading to a partial picture of the complete behavior (19, 20). Other crystallographic studies were performed with a large set of samples but without a magnetic characterization (15) or presentation of a complete magnetic characterization mainly in the high oxygen-doping region (21).

In this work we present a systematic study of varying the oxygen content of the samples and studying its influence on the structural and magnetic properties of $LaMnO_{3\pm\delta}$, covering an extensive range from 2.995 to 3.14.

## II. EXPERIMENTAL PROCEDURE

### *IIa. Sample Preparation*

A powdered sample of $LaMnO_{3\pm\delta}$ was prepared following the nitrate decomposition route. Raw materials were $La_2O_3$ (99.999%) and metallic Mn (99.99%). The raw materials were dissolved in nitric acid, and then the solution was heated until the solvent evaporated. Thereafter, annealing treatments in air with intermediate grinding were performed at 1173 and 1523 K for 24 and 6 h, respectively. The final synthesis temperature treatment was performed at 1523 K for 12 h in air.

Measurements of the equilibrium oxygen partial pressure $p(O_2)$ at constant temperature were performed using thermogravimetric equipment consisting of a symmetrical thermobalance based on a Cahn 1000 electrobalance coupled to an electrochemical system for controlling $p(O_2)$ (22). The electrochemical system—zirconia pump and oxygen sensor—(23) provides controlled $Ar–O_2$ or $CO–CO_2$ atmospheres for the thermobalance, with $p(O_2)$ values ranging from $1\times10^{-14}$ to 1 atm. Figure 1 shows the $\log(p(O_2)/\text{atm})$ vs $3\pm\delta$ curves for $LaMnO_{3\pm\delta}$ at 1173 and 1273 K. Data at 973 and 1073 K under 1 atm of oxygen were added in the plot. The absolute oxygen content of the sample was determined, adopting for the 3.00 value the inflection point of the $\log p(O_2)/\text{atm}$ vs the $3\pm\delta$ isotherm at 1273 K. The shape

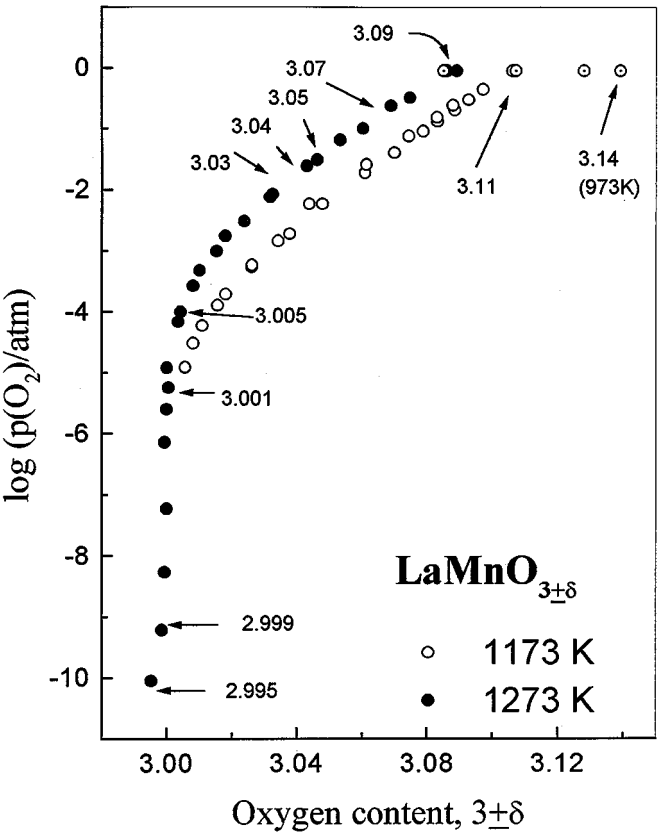


**FIG. 1.** Isotherms of $\log(pO_2)$ vs oxygen contents ($3\pm\delta$) of $LaMnO_{3\pm\delta}$ at $T=1173$ K and $T=1273$ K. Extra points under 1 atm. of oxygen at $T=973$, 1073, 1173, and 1273 K are included and marked in the plot with (●). The arrows indicate the experimental conditions used in the preparation of the samples before the quenching at 77 K.

of this isotherm indicates that $LaMnO_{3\pm\delta}$ behaves as an oxygen stoichiometric within the range $-8<\log(p(O_2)/\text{atm})<-5$. Samples with controlled oxygen contents ($2.995<3\pm\delta<3.14$) were prepared by annealing them at temperatures $T$ and $p(O_2)$ values, as indicated by arrows in Fig. 1, during 24-h periods and later quenching at liquid nitrogen temperature.

## III. RESULTS

### *IIIa. X-Ray Diffraction Results*

Powder X-ray diffraction (XRD) data were recorded on a Phillips PW 1700 diffractometer using Cu$K\alpha$ radiation and a graphite monochromator. The collection time by steps of 0.02° was 10 s. X-ray data at room temperature of the quenched samples were refined by the Rietveld method with the DBWS-9411 program (24). Secondary phases were not detected by X-ray or by SEM observations. The lattice parameters of the orthorhombic (*Pbnm* symmetry) and rhombohedral (*R3c* symmetry) structures were determined by the Rietveld method.

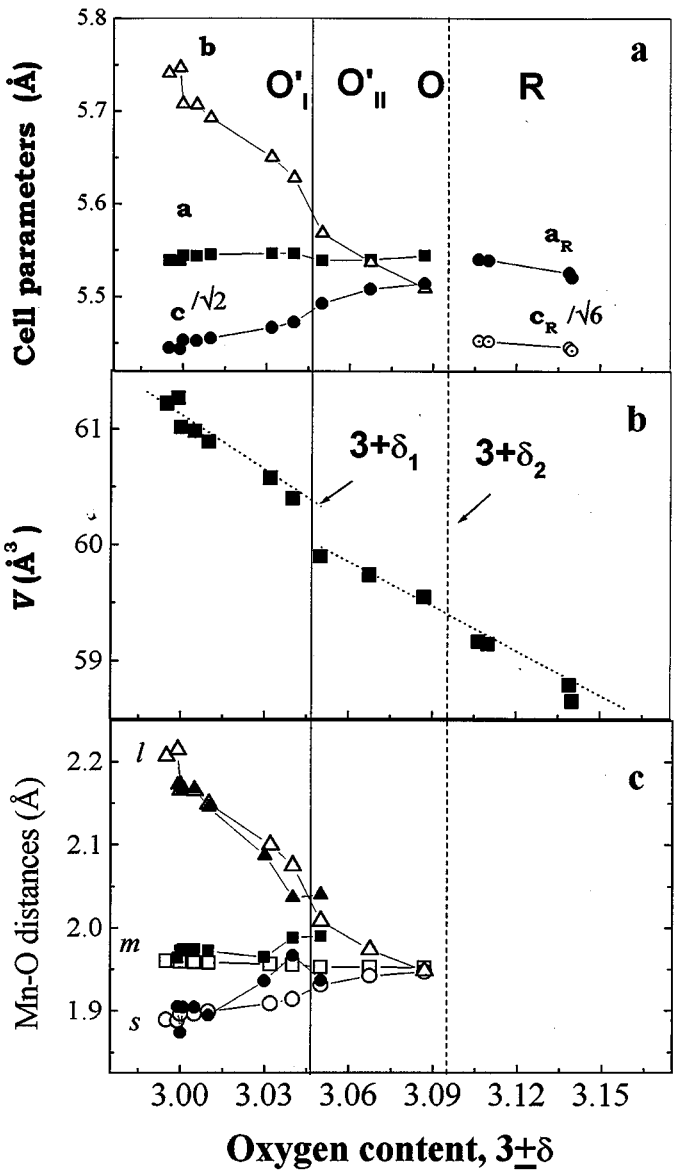


**FIG. 2.** Crystallographic characteristics of $LaMnO_{3\pm\delta}$ as a function of oxygen content. (a) Unit cell parameters, (b) variation of the unit formula volume, and (c) Mn–O distances of the surrounding oxygen octahedra. The vertical lines show the oxygen content ($3+\delta_1$ and $3+\delta_2$) where the crystallographic transitions occur.

The evolution of the lattice parameters as a function of the oxygen content ($3\pm\delta$) at room temperature is shown in Fig. 2. The static JTD diminishes continuously as the oxygen content increases until approximately a $3+\delta_1$ value between 3.04 and 3.05, as indicated by a vertical line in Fig. 2. A discontinuity in the $b$ parameter is observed between these values of oxygen content, which we use to define the transition from the $O'_I$ phase to the $O'_{II}$ phase. In the range of oxygen content less than 3.00, two deoxygenated samples (with 2.995 and 2.999) show a small discontinuity in the lattice parameters relative to that of the 3.001 sample.

Figure 2b plots the formula unit volume ($V$) as a function of oxygen content. Note the jump in the volume (1%) at $3+\delta_1$. The linear fit of $V$ vs $\delta$ for $3+\delta<3.04$ and $3+\delta>3.05$ gives the following expressions: $V(\text{Å}^3, 3+\delta<3+\delta_1) = 60.9(0.5) - 17.7(0.5)\delta$ and $V(\text{Å}^3, 3+\delta>3+\delta_1) = 60.6(0.5) - 13.7(0.7)\delta$. A linear fit including all the data points yields a value close to that reported in Ref. (25). In the next section we will discuss the different magnetic behaviors that exist below and above the $3+\delta_1$ composition.

In the bottom of Fig. 2c are shown the three different distances ($m$, $s$, $l$) between the manganese ion and the six surrounding oxygens of the octahedra. Particularly, $m$ is the distance between the Mn ion and the apical oxygen ($O_I$), and $s$ and $l$ are the short and long distances between Mn and $O_{II}$ in the $MnO_4$ plane. These distances can be computed according to the expressions proposed in Ref. (15)

$$m^2 = \frac{(a^2+b^2+c^2)}{32}, \qquad [1]$$

$$s^2 = \frac{c^2}{8} - m^2, \qquad [2]$$

$$l^2 = \frac{b^2 s^2}{16s^2 - b^2}, \qquad [3]$$

(open symbols) or by the atomic positions determined by Rietveld refinements (solid symbols). It can be seen how the deformation of the oxygen octahedra around Mn ions is reduced as the oxygen content increases.

In Ref. (21) it is mentioned that a sample with $3+\delta_2 \sim 3.07$ exhibits reflections of both O and $R$ phases and that deviations of Vegard's law occurs at both sides of this composition, suggesting the existence of a two-phase field region around this composition. However, for the 3.07 sample we have not observed the presence of a two-phase field region from the XRD measurements. At room temperature we have described the X-ray powder diffraction data for the 3.07 and 3.09 samples in the *Pbnm* symmetry and for 3.11 and 3.14 samples with the *R*3*c* symmetry group. In our case the structural transition from orthorhombic to rhombohedral at room temperature should be within the range $3.09 < 3+\delta_2 < 3.11$, which is shifted with respect to that of Ref. (21). Table 1 shows the unit cell parameters and structural symmetry found in the system.

### *IIIb. Magnetization Measurements*

The magnetic study of our samples carried out through different experiments: Magnetization ($M$) vs $T$ curves at different magnetic fields ($H$) and hysteresis loops at several temperatures. The magnetization data were taken in a commercial Quantum Design SQUID magnetometer in the

**TABLE 1**

**Structural and Magnetic Data for Different Oxygen Contents: Lattice Parameters for Orthorhombic (*a*, *b*, *c*) and Rhombohedral (*a*, *c*) Symmetries, The Number Between Parentheses Indicates the Error from the Rietveld Adjustment; Temperatures of Magnetic Order Transitions ($T_N$ and $T_C$), Curie–Weiss Temperatures (Θ); and Types of Magnetic Order (MF Indicates Magnetic Frustration). Orthorhombic Phases Are $O'_I$ with High Jahn–Teller Deformation (JTD), $O'_{II}$ with Small JTD; Both Fulfill the Criterion of the O′ Phase ($c/\sqrt{2} < a < b$) and O corresponds to $a \leq c/\sqrt{2} < b$**

| $3 \pm \delta$ | $a$ (Å) | $b$ (Å) | $c$ (Å) | Unit cell symmetry | $T_N$ or $T_C$ (K) | Θ (K) | Magnetic order |
|---|---|---|---|---|---|---|---|
| 2.995 | 5.5389(2) | 5.7411(2) | 7.7005(2) | $O'_I$-*Pbnm* | 140 | 44 | AF-WF |
| 2.999 | 5.5390(2) | 5.7472(2) | 7.6984(2) | $O'_I$-*Pbnm* | 140 | 43 | AF-WF |
| 3.005 | 5.5443(1) | 5.7078(1) | 7.7116(1) | $O'_I$-*Pbnm* | 135 | 76 | AF-WF |
| 3.010 | 5.5453(2) | 5.6927(2) | 7.7152(3) | $O'_I$-*Pbnm* | 135 | 84 | AF-WF |
| 3.03 | 5.5465(2) | 5.6504(2) | 7.7314(3) | $O'_I$-*Pbnm* | 125 | 112 | AF-WF |
| 3.04 | 5.5465(3) | 5.6280(3) | 7.7394(4) | $O'_I$-*Pbnm* | 125 | 126 | AF-WF |
| 3.05 | 5.5389(1) | 5.5683(1) | 7.7684(2) | $O'_{II}$-*Pbnm* | 120 | 145 | FM-MF |
| 3.07 | 5.5397(3) | 5.5371(3) | 7.7901(3) | $O'_{II}$-*Pbnm* | 145 | 164 | FM-MF |
| 3.09 | 5.5441(2) | 5.5093(2) | 7.798(4) | O-Pbnm | 165 | 180 | FM |
| 3.11 | 5.5391(4) | | 13.3549(7) | *R3c* | 165 | 185 | FM |
| 3.14 | 5.5209(4) | | 13.3316(7) | *R3c* | 125 | 191 | FM-MF |

$5 < T(\mathrm{K}) < 300$ temperature range. The $M$ vs $T$ curves were obtained applying a magnetic field of 5 kOe and the magnetic susceptibility ($\chi$) was computed as the ratio $M/H$. The critical temperatures, $T_C$, were determined from the maximum of $|dM/dT|$. In the magnetic ordered phase, hysteresis loops were taken between $H = -50$ kOe and $H = 50$ kOe. In some cases, at 5 K, the hysteresis loops were obtained under different conditions: (a) ZFC, the samples were cooled with $H = 0$ from a temperature above $T_C$, and (b) FC, in a similar way but cooling the samples under $H = 50$ kOe.

Magnetization curves as a function of $T$, at low magnetic fields ($H = 100$ Oe), were also carried out under ZFC and FC conditions. Before each experience, the remanent magnetic field in the SQUID was determined at 300 K in the field for which $M = 0$ and then the sample was subsequently cooled in the zero field.

Figure 3 shows the magnetization data as a function of temperature taken at 5 kOe. The magnetization at 5 K increases monotonically with $3 \pm \delta$ for $3 \pm \delta < 3 + \delta_1$ (between 2.6 and 20.5 emu/g). For $3 + \delta > 3 + \delta_1$ a jump in the magnetization values is observed, reaching a value of 51 emu/g for the $3 + \delta = 3.05$ sample.

The critical temperature decreases from $T_C \sim 140$ K, for the lower oxygen contents, to approximately 120 K for $3 + \delta = 3.03$. In the bottom panel of Fig. 3, $H/M$, taken as the inverse of the magnetic susceptibility, is also shown as a function of temperature. The Curie–Weiss temperatures (Θ) were estimated by extrapolation from the linear behavior of $H/M$ at the high-temperatures range (200–300 K). For $3 \pm \delta < 3 + \delta_1$ it can be observed that $\Theta < T_C$, while for the samples with $3 + \delta > 3 + \delta_1$, $\Theta > T_C$ as expected for a ferromagnetic material. The fact that $\Theta < T_C$ indicates that antiferromagnetic interactions are present for samples with $3 \pm \delta < 3 + \delta_1$.

To explore in more detail the magnetization response, we performed hysteresis loops at 5 K. In Fig. 4 we show four loops taken at 5 K with different oxygen content within the range $3 \pm \delta < 3 + \delta_1$. In all the cases we observe low spontaneous magnetization, a high coercive field, and nonsaturated magnetization in fields up to 50 kOe. The high coercive field ($H_C$) observed in the hysteresis loops of these samples ($3 \pm \delta < 3 + \delta_1$) is surprising and could be associated with the presence of a strong axial anisotropy. Another characteristic is the existence of an internal magnetic field ($H_i$) which produces the shift of the hysteresis loop after FC. The shift of the hysteresis loop, taken as the difference between the negative and positive values of $H_C$, is $H_i = 2300$ Oe for sample 2.995 and decreases with $3 \pm \delta$ down to a value of 400 Oe for sample 3.04. This phenomenon was observed in materials that have two phases in contact, AFM and FM, and it is called exchange anisotropy (26) or in spin glass (27). Also, we observe a small shift of the hysteresis curve along the magnetization axis; this effect was observed in samples that present some type of unidirectional anisotropy (28). The samples deficient in oxygen content, $LaMnO_{3-\delta}$, have open loops, as can be seen at a high magnetic field on the $M$–$H$ curve of the 2.995 sample in Fig. 4.

Similar hysteresis loop $T$ dependencies have been observed in the samples with $3 \pm \delta < 3 + \delta_1$. An example of this behavior is shown in Fig. 5 for the stoichiometric compound.

Differences between both sets of samples, $3 \pm \delta < 3 + \delta_1$ and $3 + \delta > 3 + \delta_1$, can be noted in the measurements of the hysteresis loops. For samples in the $3 + \delta > 3 + \delta_1$ region

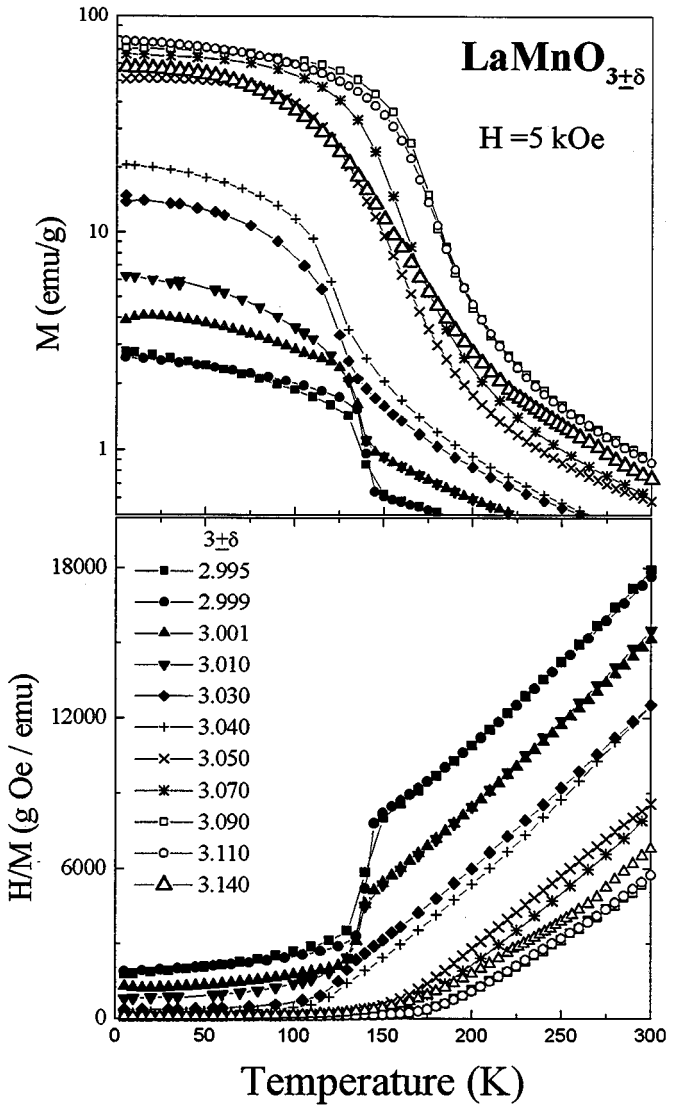


**FIG. 3.** Top: temperature dependence of magnetization for the $LaMnO_{3\pm\delta}$ samples measured at $H = 5$ kOe. Bottom: inverse of the susceptibility, taken as $H/M$, vs temperature.

the loops show low $H_C$ values, high magnetization, and a low magnetic field to reach saturation, all of which are characteristic of FM behavior. Four hysteresis loops of samples in this region are shown in Fig. 6.

In most ZFC data of $3 \pm \delta < 3 + \delta_1$ samples, measured with low $H$, an apparent negative magnetization was observed. A similar effect was also mentioned in Ref. (29). This behavior is only observed for $3 \pm \delta < 3 + \delta_1$ samples and it could be due to any small ($H \approx 2$ Oe) remanent magnetic field.

Figure 7 shows the FC and ZFC curves for $3 + \delta > 3 + \delta_1$ samples. Samples 3.05 and 3.07 display a large separation between both curves (see the upper plot of Fig. 7). This effect was attributed in Ref. (21) to a spin-glass behavior or magnetic frustration. The difference between the ZFC and FC magnetization curves in the 3.05 sample contrast with the small separation observed in the high oxygen content samples ($3 + \delta > 3.09$), which is shown in the middle and bottom plot of Fig. 7. The ZFC of the 3.14 sample grows differently from the 3.11 sample at low $T$. This behavior could be due to some type of magnetic frustration. Also in this figure it is possible to see how $T_C$ initially increases with $3 \pm \delta$ and finally decreases for higher oxygen content values ($3 + \delta = 3.14$).

Table 1 also shows the magnetic-ordering temperatures and types of magnetism found in the system.

## IV. DISCUSSION

Recently, Solovyev *et al.* (30) demonstrated the crucial role of JTD in the stability of the *A*-type AFM ground state using local spin density approximation. The lattice distortion strongly affects the anisotropic and isotropic exchange interactions in the $LaMnO_3$. In the O′ phase, the Heisemberg Hamiltonian can describe the *A*-type antiferromagnetic order:

$$\mathcal{H}_{ex} = -\frac{1}{2}\sum_{ij} J_{ij}\mathbf{S_i}\cdot\mathbf{S_j}, \qquad [4]$$

with $J_{ij} = J_{ab}$ for FM in-plane constant exchange and $J_{ij} = J_c$ for the inter-plane AFM coupling. We can estimate the values of $J_{ab}$ and $J_c$ from the measured $T_C$ and $\Theta$. Using (31)

$$T_C = \frac{2}{3}S(S+1)\frac{(4|J_{ab}| + 2|J_c|)}{k_B}, \qquad [5]$$

$$\Theta = \frac{2}{3}S(S+1)\frac{(4J_{ab} + 2J_c)}{k_B}, \qquad [6]$$

with $S = 2$. We obtained $J_{ab}/k_B = 6.5(0.8)$ K and $J_c/k = -6(1)$ K for $LaMnO_{3.00}$ as we reported in Ref. (11). For the oxidized samples in the pseudocubic ($a \approx b \approx c\sqrt{2}$) O phase, $J_{ab} \approx J_c$, see Ref. (30), and values around 10(1) K are obtained.

To describe the JTD, we define, following Solovyev *et al.* (30), a parameter $R_t = l/s$, where $l$ and $s$ are the long and short Mn–O distances computed above (see Fig. 2 and Eqs. [2] and [3]). In Fig. 8 we plot the estimated exchange constants ($J_{ab}/k_B$ and $J_c/k_B$) as a function of $R_t$. In this figure it can be seen that $J_c/k_B$ goes to zero at $\delta_1$.

In a two sublattice magnetization model, with $\mathbf{M_i} = g\mu_B\langle\mathbf{S_i}\rangle$ ($i = 1, 2$), the antisymmetric and anisotropic Dzialoshinski–Moriya (D–M) coupling mentioned in the Introduction is responsible for the canting of the magnetizations. The corresponding energy term is

$$\mathcal{H}_{DM} = \sum_{i<j}\mathbf{D_{ij}}\cdot\mathbf{S_i}\times\mathbf{S_j} \qquad [7]$$

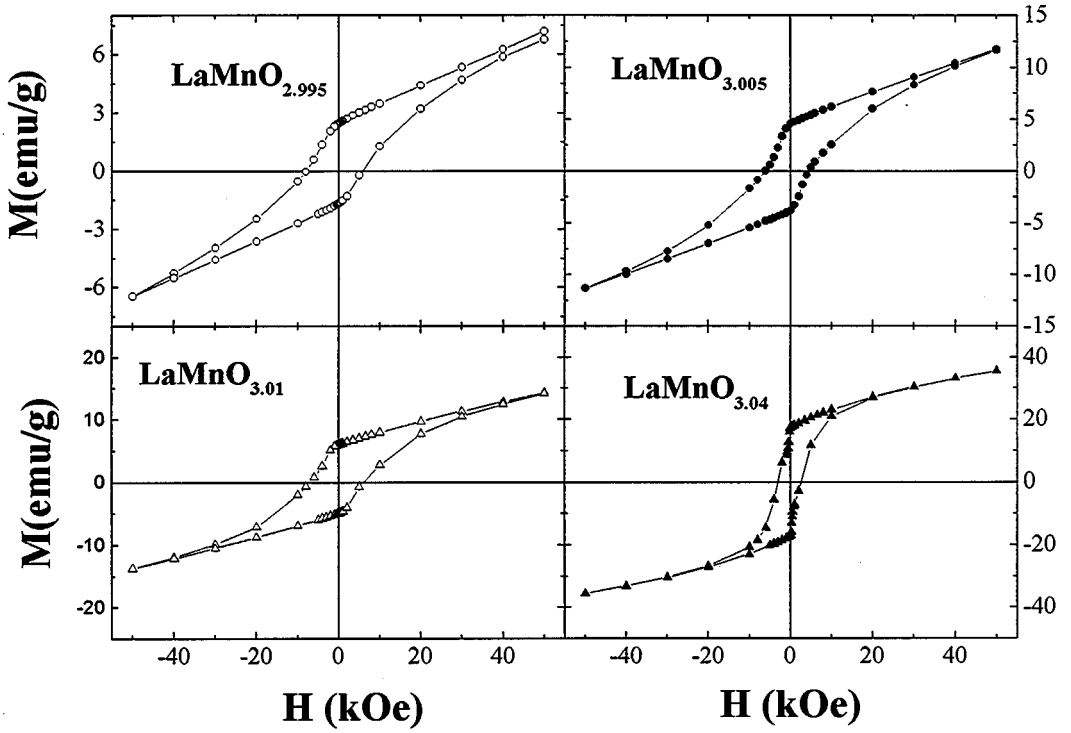


**FIG. 4.** Hysteresis loops of $LaMnO_{3\pm\delta}$ taken at $T = 5$ K, after cooling with a magnetic field of $H = 50$ kOe, for samples with $3 \pm \delta < 3 + \delta_1$ in the weak ferromagnetic region.

For $T < T_C$, in a weak ferromagnetic material, $M$ is linear with $H$ at high magnetic fields. In this case $M(T, H) = m_0(T) + \chi_{HF}(T)H$, where $m_0$ is the magnetization at zero magnetic field and $\chi_{HF} = \chi_{AF}$ is the susceptibility corresponding to the AFM interactions.

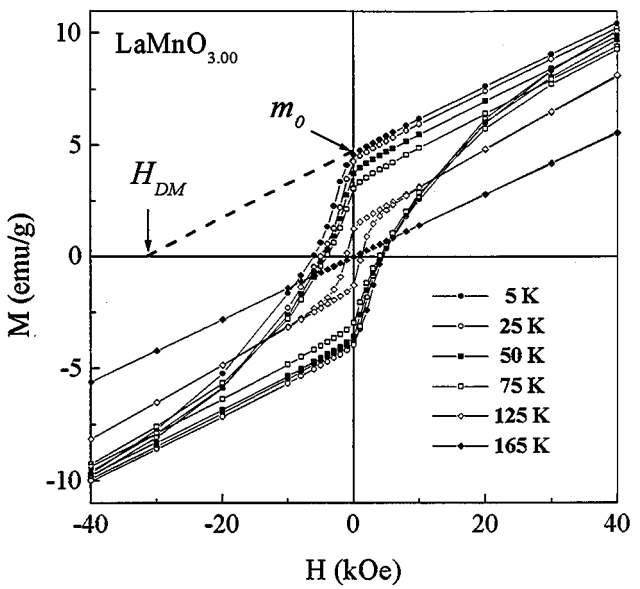


**FIG. 5.** Hysteresis loops at different temperatures for a stoichiometric sample of $LaMnO_3$. Arrows indicate the weak ferromagnetic parameters: $m_0$ and $H_{DM}$.

Using an effective exchange constant ($\lambda \propto 1/\chi_{HF} \propto J_c$) to describe the AFM coupling between the two magnetizations, and the Dzyalohinski–Moriya vector (**D**) perpendicular to the mgnetization plane, $m_0 \approx DM_S/\lambda$ is the ferromagnetic component coming from the canting of the magnetization. We obtain $DM_S = H_{DM}$ by extrapolation of the magnetization data down to the $H$ axis as shown in Fig. 5 ($H_{DM} \approx 33$ kOe at 5 K in $LaMnO_{3.00}$). If we consider an experimental value of $M_S \cong 3.5\,\mu_B$ (19), then $D = 0.7(0.1)$ K, which is in excellent agreement with the $D$ value obtained from EPR measurements (32).

According to this picture, we take $m_0$ and $\chi_{HF}$ from the hysteresis loops at each temperature for the other oxygen contents. Figure 9a shows how $m_0$ decreases with increasing $T$ until $T_C$. For $T > T_C$, in the paramagnetic phase, $m_0 = 0$. Also, the weak FM component increases with $\delta$. $H_{DM}$ increases from 27 kOe in the 2.995 sample to 75 kOe in the 3.04 sample. The canting angle between the spins can be calculated as $\alpha = m_0/2M_S$, and it goes from 0.02° (2.995) to 0.13° (3.04).

Figure 9b shows $\chi_{HF}$ as a function of $T$ for different oxygen content samples. All of them show similar behavior: for $T \ll T_C$, we observed constant values, and near $T_C$, $\chi_{HF}$ rises to a maximum and then drops quickly, illustrating

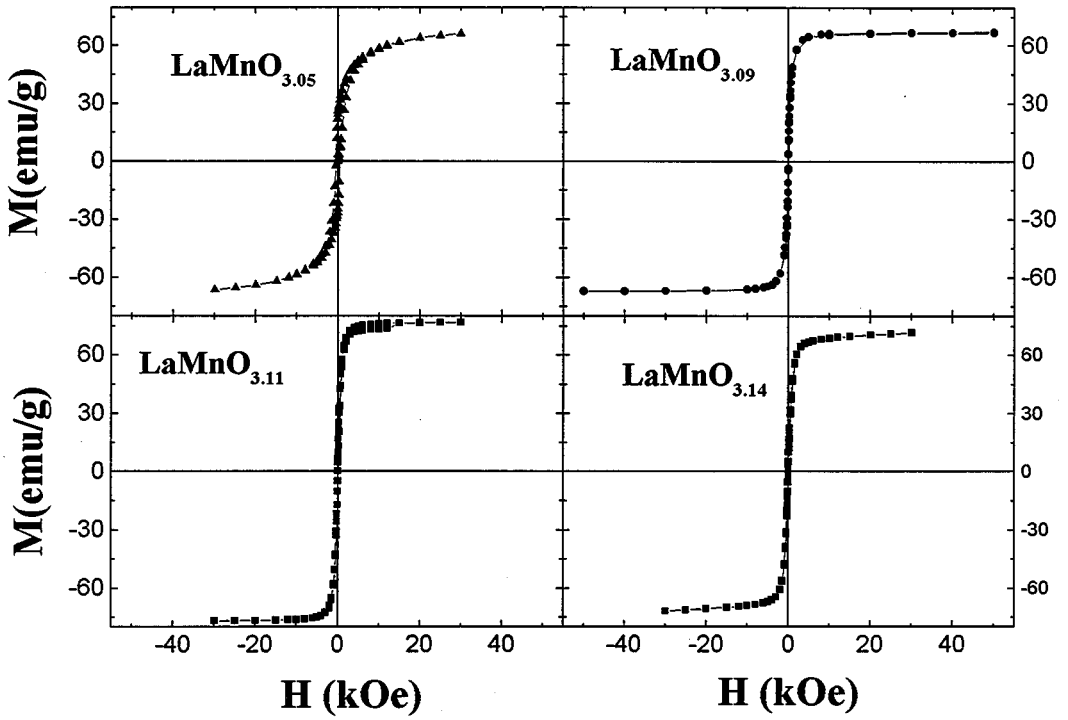


**FIG. 6.** Hysteresis loops of $LaMnO_{3\pm\delta}$ taken at $T = 5$ K, after cooling with a magnetic field of $H = 50$ kOe, for samples with $3+\delta > 3+\delta_1$ in the ferromagnetic region.

the antiferromagnetic susceptibility of the material. At low temperatures $\chi_{HF}$ increases with $3+\delta$, which is consistent with the tendency observed in the exchange constant shown in Fig. 8 ($\chi_{HF} \propto 1/|J_c|$). Also, we obtain a constant value of 0.8 for the ratio of the susceptibility at 5 K relative to the maximum susceptibility values ($\chi_{HF}(5\text{ K})/\chi_{HF}(T)_{max} = 0.8$), which is near the 0.7 value expected according to the mean field theory.

For a complete magnetic picture, it is necessary to add an extra energy term $\mathscr{H}_A$ that includes the crystalline anisotropy, responsible for magnetic moments laying along the "**c**" axis. We may also include other sources of anisotropy that could explain the unidirectional and/or exchange anisotropy observed.

For $3\pm\delta < 3+\delta_1$ samples, we conclude that the small ferromagnetic contribution observed comes from a magnetic canted structure. Our results are in agreement with a recent neutron diffraction study by Ritter *et al.* (19). They reported, for a $3+\delta = 3.025$ ($< 3+\delta_1$) sample that AFM and FM contributions appear at the same temperature. This suggests the existence of a low-temperature AFM canted structure.

A summary of the main magnetic properties is displayed in Fig. 10. In part "a" are plotted the Curie–Weiss temperature ($\Theta$) and the magnetic-ordering temperature ($T_N$ for AFM or $T_C$ for FM) as a function of the oxygen content. For $3\pm\delta < 3+\delta_1$, $\Theta$ is lower than $T_N$ and it increases with $3\pm\delta$, reaching the $T_N$ value for $3+\delta = 3+\delta_1$, which corresponds to the jump in the unit formula volume, and separates the AFM and FM regions. For a higher oxygen content ($3+\delta > 3+\delta_1$) $\Theta$ is higher than $T_C$. Deviation of a Curie–Weiss law observed (Fig. 3) are an actual subject of discussion and some authors propose the existence of magnetic polarons (33, 34). In this region double-exchange mechanism plays an important role, but analyses of this is out of the scope of this work.

Figure 10b shows the coercive fields at 5 K as a function of the oxygen content. Clearly, it can be seen that the weak ferromagnetic samples present high coercive fields except for the 2.999 sample. The saturated magnetic moment at 5 K is shown in Fig. 10c; the $3+\delta_1$ value also marks the differences between both groups of samples in the $LaMnO_{3\pm\delta}$ system. In the low-temperature range, for $3+\delta > 3+\delta_1$, the magnetization increases continuously with $3+\delta$ until it reaches the maximum value for the 3.11 sample. In Fig. 9c it can be observed that for high $3+\delta$ values ($3+\delta \sim 3.14$) the magnetization saturation decreases below the expected value for a complete ferromagnetic alignment of the magnetic moments. This effect was reported in Ref. (19, 21) and it has been explained being due to the large amount of cationic vacancies present in the sample which break the ferromagnetic path between the Mn ions.

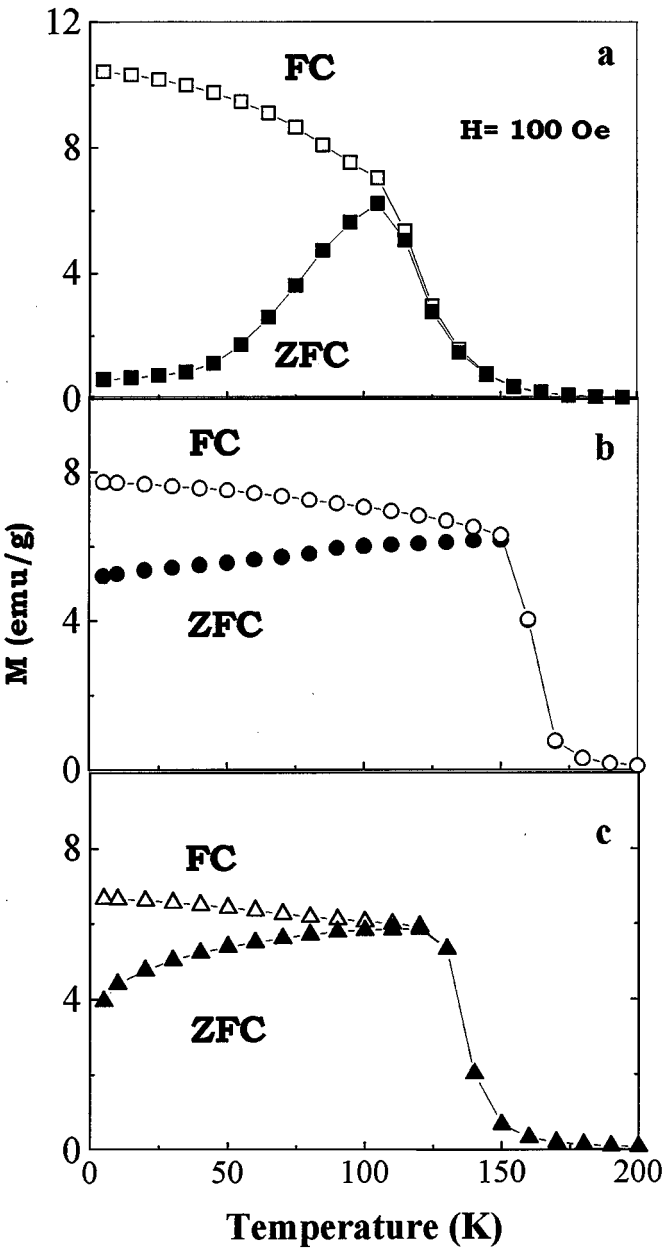


**FIG. 7.** Thermal dependence of the ZFC and FC magnetization taken at $H = 100$ Oe for $LaMnO_{3\pm\delta}$ in the ferromagnetic region, $(3+\delta > 3+\delta_1)$: (a) $LaMnO_{3.05}$; (b) $LaMnO_{3.11}$; (c) $LaMnO_{3.14}$.

## V. CONCLUSIONS

1. $LaMnO_{3\pm\delta}$ samples with different oxygen contents have been prepared by annealing at high temperatures under different $p(O_2)$ and subsequent quenching to 77 K, studying the structural and its magnetic properties. Our attention was focused on the low oxygen content values.

2. $LaMnO_{3\pm\delta}$ samples within the range $2.995 < 3\pm\delta < 3.04$ exhibit a highly distorted orthorhombic phase ($O'_I$) at room temperature. Antiferromagnetic order is dominant at low temperatures with a small canting of the magnetic moments. This canting increases with the oxygen content with the consequent enhancement of the magnetization. The Curie–Weiss temperature, lower than $T_N$, increases with $3\pm\delta$ until $T_N$ is reached and then it increases monotonically. A crossover of $\Theta$ and $T_N$ occurs at $3+\delta_1$. The high-field magnetic susceptibility shows the typical behavior of an AFM material. These weak ferromagnetic samples show hysteresis loops with high coercive fields. These loops are shifted for the measurements performed under FC conditions due to the appearance of an unidirectional anisotropy. This effect is more noticeable for $LaMnO_{3-\delta}$ samples. An extra characteristic of these oxygen-deficient samples is the existence of open hysteresis loops. The exchange and Dzialoshinski–Moriya constants and the canting angles were computed for different oxygen contents.

3. $LaMnO_{3+\delta}$ within $3+\delta_1 < 3+\delta < 3+\delta_2$ show high magnetization values, ferromagnetic behavior, and small coercive fields. The samples have a less distorted crystallographic lattice ($O'_{II}$ phase and O phase) with a marked difference between the ZFC and FC magnetization curves, suggesting some degree of magnetic frustration.

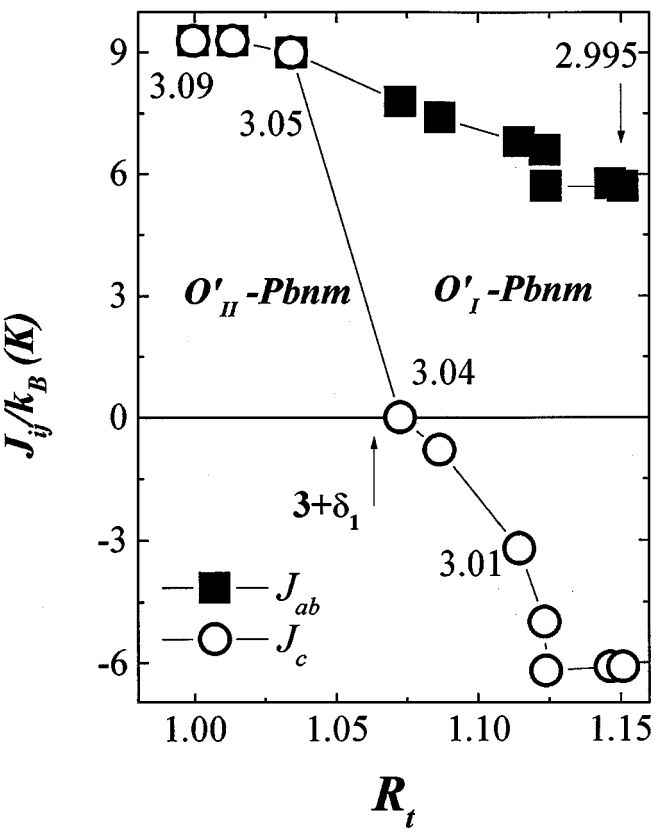


**FIG. 8.** Exchange constants ($J_{ab}$ and $J_c$) as a function of $R_t$, the $MnO_4$ plane distortion.

4. $LaMnO_{3+\delta}$, with $3+\delta > 3+\delta_2$, exhibit rhombohedral symmetry and ferromagnetic characteristics, and the ZFC and FC magnetization curves present small differences between them. For higher oxygen compositions the saturation magnetization is less than that in the $3+\delta \approx 3+\delta_2$ sample.

5. It is clear from the present work that an evolution from an antiferromagnetic region, with a large cooperative Jahn–Teller deformation ($O'_I$) to a ferromagnetic one, with small distortions ($O'_{II}$), is characterized by a discontinuous change of the unit cell volume. The ferromagnetism is reached without the Jahn–Teller deformation disappearing totally or the structural criterion O ($a \leq c/\sqrt{2} < b$) being fulfilled.

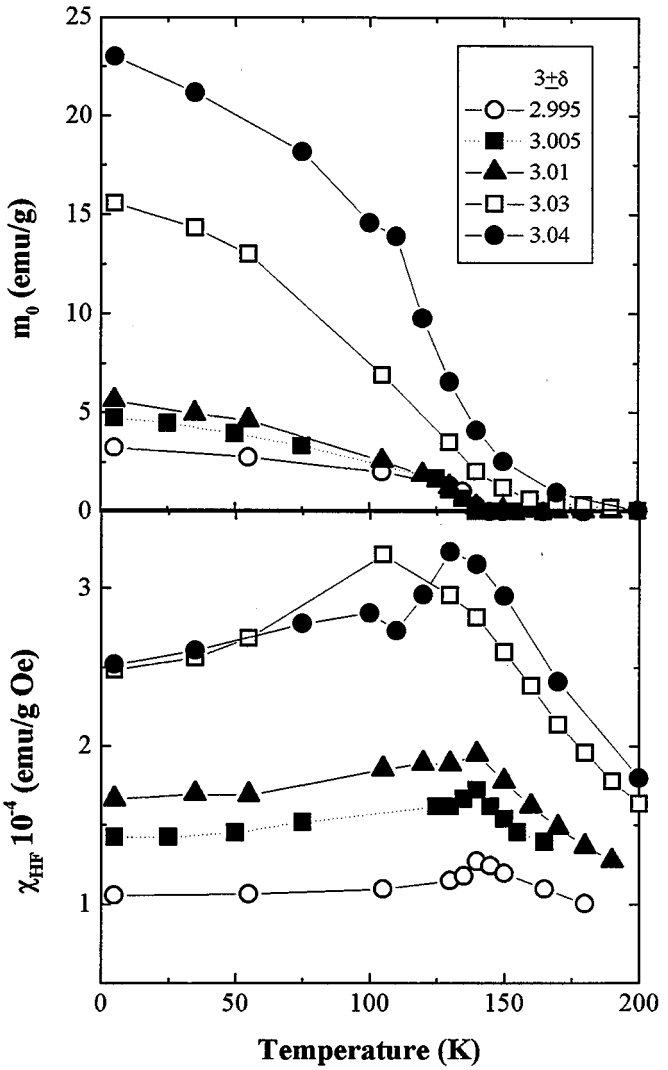


**FIG. 9.** Top: extrapolated magnetization to zero field, $m_0$ vs $T$. Bottom: Magnetic susceptibility at high field, $\chi_{HF}$ vs $T$.

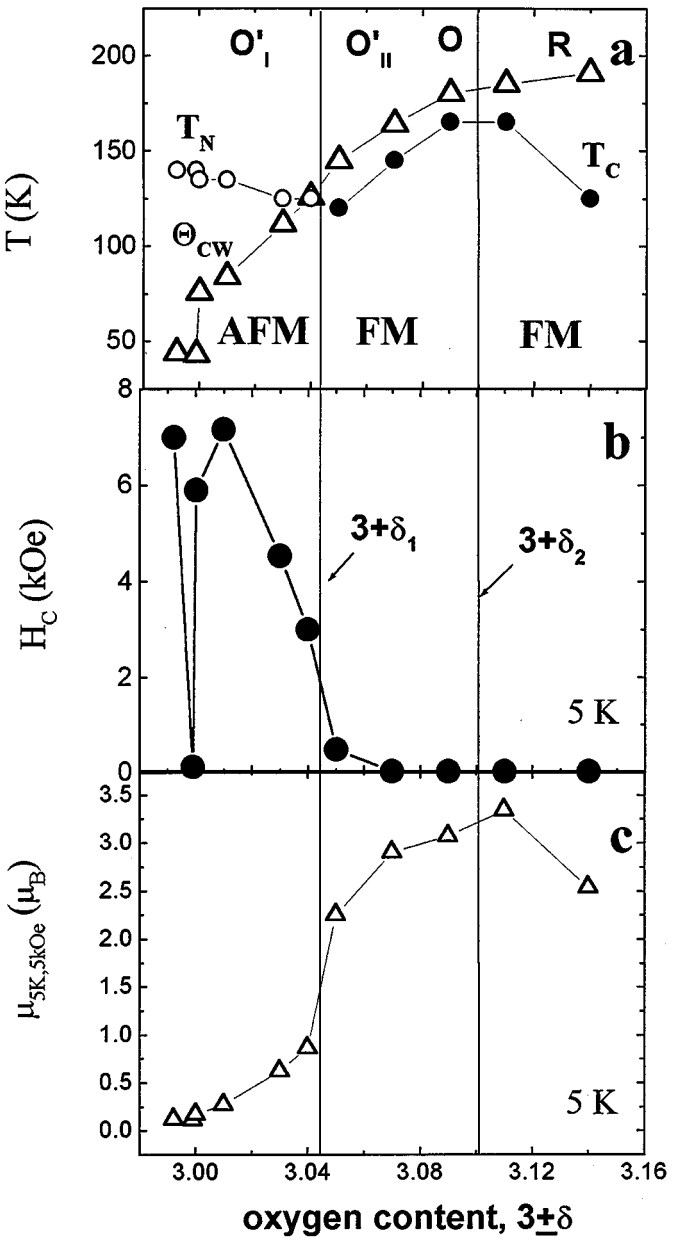


**FIG. 10.** Magnetic parameters of $LaMnO_{3\pm\delta}$ as a function of the oxygen content. (a) Curie–Weiss ($\Theta$), Néel ($T_N$), and Curie ($T_C$) temperatures; (b) coercive field obtained from the hysteresis loops at $T = 5$ K; (c) saturation magnetic moments at $T = 5$ K. The vertical lines show the oxygen contents ($3+\delta_1$ and $3+\delta_2$) where the crystallographic transitions occur.

## ACKNOWLEDGMENTS

The authors gratefully acknowledge the help of Dr. V. Grünfeld in the English revision and Dr. C. Ramos for the critical reading of this manuscript. This work was supported by CNEA (Argentine Atomic Energy Commission), CONICET (Argentine National Research Council), Fundación Antorchas, CEB (Bariloche Electricity Company), and CEE (Commission of the European Communities) through DGXII Contract CII*CT92-0087.

## REFERENCES


1. R. von Helmolt, J. Wecker, B. Holzapfel, L. Schultz, and K. Samwer, *Phys. Rev. Lett*. **71,** 2331 (1993).
2. S. Jin, T. H. Tiefel, M. McCormark, R. A. Fastnacht, L. H. Chen, and R. Ramesh, *Science* **264,** 413 (1994).
3. C. Zener, *Phys. Rev*. **82,** 403 (1951).
4. P. W. Anderson and H. Hasegawa, *Phys. Rev*. **100,** 675 (1955).
5. P. G. de Gennes, *Phys. Rev*. **181,** 141 (1960).
6. G. H. Jonker and J. H. Van Santen, *Physica* **16,** 337 (1950).
7. A. J. Millis, P. B. Littlewood, and B. I. Shraiman, *Phys. Rev. Lett*. **74,** 5144 (1995).
8. A. J. Millis, B. I. Shraiman, and R. Mueller, *Phys. Rev. Lett*. **77,** 175 (1996).
9. E. O. Wollan and W. C. Koehler, *Phys. Rev*. **100,** 545 (1955).
10. J. B. Goodenough, *Phys. Rev*. **100,** 564 (1955).
11. M. T. Causa, G. Alejandro, R. Zysler, F. Prado, A. Caneiro, and M. Tovar, *J. Magn. Magn. Mater*. **196–197,** 506 (1999).
12. F. Prado, R. Zysler, L. Morales, A. Caneiro, M. Tovar, and M. T. Causa; *J. Magn. Magn. Mater*. **196–197,** 481 (1999).
13. P. Norby, I. G. Krogh Andersen, E. Krogh Andersen, and N. H. Andersen, *J. Solid State Chem.* **119,** 191 (1995).
14. J. Goodenough, A. Wold, R. J. Arnott, and N. Menyuk, *Phys. Rev*. **124,** 373 (1961).
15. A. K. Bogush, V. I. Pavlov, and L. V. Balyko, *Cryst. Res. Technol.* **18,** 589 (1983).
16. J. Inoue and S. Maekawa, *Phys. Rev. Lett*. **74,** 3407 (1995).
17. A. Wold and R. J. Arnott, *J. Phys. Chem Solids* **9,** 176 (1959).
18. J. A. M. Van Roosmalen and E. H. P. Cordfunke, *J. Solid State Chem.* **110,** 109 (1994).
19. C. Ritter, M. R. Ibarra, J. M. De Teresa, P. A. Algarabel, C. Marquina, J. Blasco, J. García, S. B. Oseroff, and S. W. Cheong, *Phys. Rev. B* **56,** 8902 (1997).
20. Q. Huang, A. Santoro, J. W. Lynn, R. W. Erwin, J. A. Borchers, J. L. Peng, and R. L. Greene, *Phys. Rev. B* **55,** 14987 (1997).
21. J. Töpfer and J. B. Goodenough, *J. Solid State Chem.* **130,** 117 (1997).
22. A. Caneiro, P. Bavdaz, J. Fouletier, and J. P. Abriata, *Rev. Sci. Instrum.* **53,** 1072 (1982).
23. A. Caneiro, M. Bonat, and J. Fouletier, *J. Appl. Electrochem.* **11,** 83 (1981).
24. R. A. Young, A. Sakthivel, T. S. Moss, and C. O. Paiva-Santos, *J. Appl. Crystallogr.* **28,** 366 (1995).
25. J. A. M. Van Roosmalen, P. van Vlaanderen, E. H. P. Cordfunke, W. L. Ijdo, and D. J. W. Ijdo, *J. Solid State Chem.* **114,** 516 (1995).
26. I. S. Jacobs and C. P. Bean, Fine particles, thin films and exchange anisotropy, *in* "Magnetism," (G. T. Rado and H. Suhl, Eds.), Vol. III, Chap. 6, Academic Press, New York, 1963. For a review, see W. H. Meiklejhon, *J. Appl. Phys.* **33,** 1328 (1962).
27. K. Binder and A. P. Young, *Rev. Mod. Phys.* **58,** 801 (1986).
28. G. Matsumoto, *J. Phys. Soc. Jpn.* **29,** 606 (1970).
29. B. C. Hauback, H. Fjellvåg, and N. Sakai, *J. Solid State Chem.* **124,** 43 (1996).
30. I. Solovyev, N. Hamada, and K. Terakura, *Phys. Rev. Lett*. **76,** 4825 (1996).
31. A. Herpin, "Theorie du Magnétisme." Presses Universitaires, Grenoble, 1968.
32. M. Tovar, G. Alejandro, A. Butera, A. Caneiro, M. T. Causa, F. Prado, and R. D. Sánchez, to be published.
33. J. M. de Teresa, M. R. Ibarra, P. A. Algarabel, C. Ritter, C. Marquina, J. Blasco, J. García, A. del Moral, and Z. Arnold, *Nature* **386,** 256 (1997).
34. M. Hennion, F. Moussa, J. Rodriguez-Carvajal, L. Pinsard, and A. Revcolevschi, *Phys. Rev. B* **56,** 497 (1997). M. Hennion, F. Moussa, G. Bioteauu, J. Rodriguez-Carvajal, L. Pinsard, and A. Revcolevschi, *Phys. Rev. Lett*. **81,** 1957 (1998).